Journal of Polymer Science

WILEY

JOURNAL OF POLYMER SCIENCE

RESEARCH ARTICLE OPEN ACCESS

Recycling-Induced Changes of Molecular Weight and Structural Properties in PET Monopolymer Blends

Florian Stephan[1] | Justus Friedrich Thümmler[2] | Wolfgang Hubertus Binder[2] | Holger Ruckdäschel[1,3]

[1]Department of Polymer Engineering, University of Bayreuth, Bayreuth, Germany | [2]Institute of Chemistry, Faculty of Natural Sciences II, Martin Luther University Halle-Wittenberg, Halle, Germany | [3]Neue Materialien Bayreuth GmbH, Bayreuth, Germany

Correspondence: Holger Ruckdäschel (ruckdaeschel@uni-bayreuth.de)

Received: 6 November 2025 | **Revised:** 9 March 2026 | **Accepted:** 24 March 2026

Keywords: mechanical properties | molecular weight distribution | monopolymer blend | PET | rheology | twin-screw extrusion

ABSTRACT

Mechanical recycling of plastics is the most common process, but mixed polymer chain lengths make molecular weight effects unclear. By blending high and low molecular weight (M_w) Polyethylene terephthalate (PET), we want to investigate the changes in molecular weight distribution in the extrusion process and the properties regarding processability and performance. Bottle-grade PET (high M_w) and fiber-grade PET (low M_w) were used. The aim of the study was to understand the structure–property relationship relevant to mechanical recycling for PET. We focused on melt viscosity, degree of crystallinity, tensile strength, and elongation at break, all strongly dependent on molecular weight. Different blend ratios were extruded and tested for molecular weight, thermal, rheological, and mechanical behavior. The results show that blending enables precise tuning of properties. GPC and rheology confirm chain scission and extension during extrusion, leading to convergence of molecular weight distributions. Thermal analysis shows a reduced degree of crystallinity and melting temperature with higher M_w. Mechanical tests reveal that higher M_w improves tensile strength and elongation up to a threshold. All blends show similar molecular weight distribution, ensuring consistent properties and wider processing options for recycled PET.

1 | Introduction

Plastics are important in modern life. These materials are versatile and are used in a variety of sectors. These sectors include packaging, textiles, construction, medicine, automotive, aviation, electronics, leisure and sports goods, and energy [1]. Polyethylene terephthalate (PET) is a thermoplastic polyester that combines high strength and stiffness, chemical resistance and, depending on additives and processing, transparency. PET is also suitable for weather-resistant applications and has an effective barrier against gases such as oxygen and carbon dioxide, a property that can be further enhanced through biaxial stretching [2, 3]. These characteristics make PET particularly well-suited for applications such as bottles containing carbonated beverages, where gas retention and material durability are essential [4]. Polyethylene terephthalate is one of the most produced plastics on the global market [5]. The primary applications of this material are packaging, particularly in the context of bottles and technical applications, such as in the electrical and electronics industry, as well as in glass fiber-reinforced compounds [3, 6]. A further range of potential applications has been identified in the domains of textiles, medical products and construction [7–9].

The release of plastics such as PET into the environment through landfills or mismanagement has a significant impact. Microplastics impact marine, terrestrial and coastal ecosystems, exhibit toxic effects, interfere with nutrient cycles and pose a threat to various forms of life [10, 11]. To mitigate these consequences, it is crucial to transition from a linear to a circular economy. The aim is to minimize plastic waste and stop it accumulating in landfill sites [12].

Plastic recycling involves primary (closed loop), secondary (downcycling), tertiary (chemical monomer recovery), and secondary (energy recovery) methods [12]. Mechanical recycling, which includes both, primary and secondary recycling processes, involves shredding, cleaning, and subsequent regranulation of sorted plastic waste. Regranulation typically takes place after twin-screw extrusion at elevated temperature and pressure. In order to enhance the material properties of the recyclate, it is common to incorporate polymer blends, additives, stabilizers, or fillers during the processing stage [13–15]. One major drawback of mechanical recycling is molecular weight degradation. Machine Learning has recently been recognized as a promising approach to optimize thermoplastic recycling processes [16].

The degradation mechanisms of PET during processing can be divided into three main categories: hydrolytic degradation, thermal degradation, and thermal-oxidative degradation. Hydrolytic degradation occurs at temperatures above 100°C. It is caused by moisture as an autocatalytic reaction in which water breaks down ester bonds. This leads to an increase in hydroxyl and carboxyl end groups [17]. In contrast, thermal degradation occurs at high temperatures in the absence of oxygen through random chain scissions at ester bonds. This produces vinyl and carboxyl end groups [17]. This process is particularly relevant in the molten state, at temperatures above 270°C [18]. Thermal-oxidative degradation occurs at temperatures above 180°C–200°C in the presence of oxygen. It proceeds via radical mechanisms, leading to chain breaks and the formation of hydroperoxides. Depending on the oxygen content, branching can occur [19].

The material's rheological, thermal and mechanical properties are negatively affected [20, 21]. As a result, downcycling often occurs, leading to the use of the material for applications with lower requirements and a reduction in the overall quality of the reprocessed material compared to its original form [22]. A significant decrease in viscosity can already be observed after the first recycling cycle, whereas mechanical properties tend to decline only slightly [23, 24]. Additionally, the glass transition temperature (T_g) of PET is affected by its molecular weight. As molecular weight decreases, chain mobility increases, resulting in a reduction in T_g [25].

Although chemical and enzymatic recycling processes such as glycolysis and enzymatic depolymerization can recover high-quality monomers, they are technically complex and costly [26–30]. Challenges related to scalability and economic viability remain, which complicates large-scale implementation [31, 32]. Therefore, optimizing mechanical recycling is crucial for the transition to a circular economy.

One promising approach to compensate for the negative effects of molecular weight degradation is to blend recycled PET with virgin material. Studies show that mechanical and rheological properties can be significantly improved by appropriate blending ratios [33–36]. Fann et al. investigated such virgin/recycled PET blends and found that mechanical properties and degree of crystallinity increase with increasing recycled polymer content as the crystallization behavior is influenced [37]. In contrast, Lee et al. showed that both thermal stability and mechanical properties can be improved by increasing the virgin content [38]. Elamri et al. analyzed fibers made from mixtures of virgin and recycled PET. He observed that as the proportion of virgin PET increased, the breaking stress increased linearly and the elongation at break decreased linearly. The zero shear viscosity of all blends is lower than predicted by the logarithmic rule [39].

Variations in recyclate quality, processing conditions and additive formulations contribute to inconsistencies in the literature and complicate direct comparisons between studies [40]. To use recycled PET for high-quality applications, it is crucial to have a solid understanding of how molecular weight influences important properties relevant to processability and performance. Examples of such properties include melt viscosity, degree of crystallinity, tensile strength, and elongation at break. Mixing PET with different M_w reflects the reality of recycling, as waste typically has different M_w values. At the same time, mixing low and high M_w PET allows the properties to be specifically adjusted for use in high-quality products.

This study therefore aims to improve the understanding of monopolymer blends by systematically blending low and high molecular weight PET grades. The work investigates how blending affects the molecular weight distribution as well as the thermal, rheological, and mechanical properties. The results are particularly relevant for recycling scenarios in which different M_w of plastic waste are extruded and where recycled PET generally has a lower molecular weight than new material. This adjustment of the M_w also changes the properties. By providing a deeper understanding of the structure–property relationships in such blends, this study aims to enable the targeted use of recycled materials in high-performance applications.

2 | Materials and Methods

2.1 | Materials

The PET grades used in this study have different intrinsic viscosities (IV) and therefore different molecular weights (M_w). The low IV PET is TRN-MJ from Teijin Ltd. (Tokyo, Japan) and is mainly used for injection molding applications or fibers. The PET with the high IV is NEOPET84 from the NeoGroup (Klaipėda, Lithuania) and is used for applications such as beverage bottles or films. The IV values presented in Table 1 were obtained from manufacturer data sheets. The experimental determination of the number-average molecular weight (M_n), weight-average molecular weight (M_w), and polydispersity index (PDI) is also shown.

2.2 | Compounding and Sample Preparation

The PET grades were molten and blended in a co-rotating, intermeshing twin-screw extruder ZSK 26MC from Coperion GmbH (Stuttgart, Germany). The screw configuration is shown in Figure 1 and is a typical combination of conveying, shearing and mixing elements. The Supporting Information provides a technical description of the screw elements. The color coding of the elements corresponds to the technical specifications in Figures S1–S11 of the Supporting Information. The screw diameter was 25.5 mm and has a length-to-diameter ratio (L/D ratio)

TABLE 1 | Properties of virgin blend components.

Material	Intrinsic viscosity IV (dL/g)	Number-average molecular weight M_n (g/mol)	Weight-average molecular weight M_w (g/mol)	Polydispersity index (PDI)
TRN-MTJ	0.53	20,600	47,500	2.3
NEOPET84	0.84	31,300	81,100	2.6

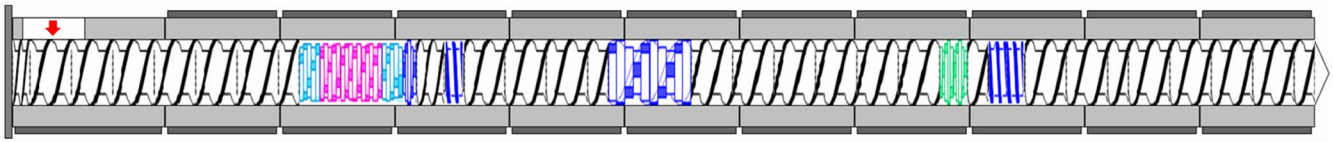

FIGURE 1 | Modular screw configuration with elements along the screw axis: Conveying elements, kneading blocks, and mixing elements. The color coding of the screw elements corresponds to the technical specifications provided in the Supporting Information.

TABLE 2 | Overview of all blends and their components.

Sample name	TRN-MTJ (low IV) (wt.%)	NEOPET84 (high IV) (wt.%)
100/0	100	0
80/20	80	20
60/40	60	40
50/50	50	50
40/60	40	60
20/80	20	80
0/100	0	100

of 44. The material was processed at a throughput of 10 kg/h. The process parameters for the extrusion were a temperature profile of 10 heating zones (80/80/240/260/260/260/260/260/260/260 in °C) and a screw speed of 300 rpm (revolutions per minute). The residence time was determined by modeling the behavior of a co-rotating twin-screw extruder using SIGMA simulation software [41]. The calculated average residence time is 150 s.

The samples for the rheological tests were produced using a hot press (P/O/Weber GmbH, Remshalden, Germany). The geometry of the specimens was disc-shaped, with a diameter of 25 mm and a thickness of 1.2 mm. The samples for the mechanical tests were produced using an injection molding machine (ARBURG GmbH + Co KG, Loßburg, Germany). For the tensile tests, ISO 527-1A type specimens were used, with dimensions of 170 mm length, 10 mm width (narrow section), and 4 mm thickness. To minimize the influence of variations in the degree of crystallinity variations across the cross-section of the blends on their mechanical properties, all samples were annealed at 150°C for 5 min in a hot press without applying pressure prior to testing.

To avoid degradation by hydrolysis, the granules and the prepared sample were dried at 120°C under vacuum for at least 15 h before processing and measurements. An overview of all blends and their composition is shown in Table 2.

2.3 | Molecular Weight Analysis

A hexafluoroisopropanol (HFIP) -based gel permeation chromatography (GPC) measurements were performed at 20°C with 0.1 mol/L KTFAc (potassium trifluoroacetate) on a Viscotek GPCmax VE 2001 from Malvern applying a PSS PFG precolumn and a PSS PFG main column. The solvent was an HFIP solution with 0.1 mol/L KTFAc and the sample concentration was adjusted to approximately 3 mg/mL at a flow rate of 0.5 mL/min. The refractive index was determined using a VE 3580 RI (Refractive Index) detector from Viscotek. External calibration was performed using polymethyl methacrylate (PMMA) standards (purchased from PSS) with a molecular weight range from 602 to 182,000 g/mol. OmniSEC software (Version 5.12.) was used to evaluate the data.

2.4 | Thermal Behavior

The thermal properties of all samples were analyzed using a dynamic differential scanning calorimeter (DSC 1, Mettler Toledo, Columbus, OH, USA). Measurements were conducted under a nitrogen atmosphere, with sample masses ranging from 5 to 10 mg.

For thermal characterization, the DSC temperature program included two heating cycles and one cooling cycle between 25°C and 300°C at a constant rate of 10 K/min. A 2-min isothermal hold was performed at 300°C after the first heating and at 25°C after the cooling step.

To determine the degree of crystallinity of the annealed tensile bars, specimens were cut out from the core of the tensile test samples and subjected to a separate heating cycle from 25°C to 300°C at a heating rate of 10 K/min.

Data analysis was performed using STARe software (Mettler-Toledo AG, Schwerzenbach, Switzerland). The degree of crystallinity was quantified based on the melting enthalpy (ΔH_m),

which was determined by integrating the area under the endothermic melting peak in the second heating curve using a linear baseline. The measured melting enthalpy (ΔH_m) was compared to the theoretical melting enthalpy of fully crystalline PET ($\Delta H_m = 140\,J/g$) [42].

2.5 | Rheological Behavior

Shear rheology experiments were conducted in oscillatory mode using an Anton Paar MCR 702 rheometer (Graz, Austria) at 270°C to determine the viscous and elastic material parameters. Measurements were performed in a plate-plate geometry with a plate diameter of 25 mm and a gap of 1 mm. Strain sweeps were first conducted to identify the linear viscoelastic region (LVR) before proceeding with frequency sweeps. Subsequently, frequency sweeps were carried out under Small Amplitude Oscillatory Shear (SAOS) at a constant strain of 5% within the LVR, covering an angular frequency range from 1 to 500 rad/s.

To analyze the flow behavior of the blends studied, the shear viscosity data were fitted using the Carreau-Yasuda model (Equation 1), which describes the relationship between viscosity and shear rate [43].

$$\eta(\dot{\gamma}) = \eta_\infty + \left(\eta_0 - \eta_\infty\right) \cdot \left[1 + (\lambda \cdot \dot{\gamma})^a\right]^{\frac{n-1}{a}} \quad (1)$$

Following the observations made by Cox and Merz, the steady shear viscosity was equated to the magnitude of the complex viscosity at the corresponding frequencies [44]. The Cox Merz rule is applicable to PET [45]. The model parameters η_0 and η_∞, represent the zero and infinite shear viscosity, λ represents a characteristic relaxation time, a characterizes the width of the transition region and n the shear thinning exponent, respectively.

2.6 | Mechanical Behavior

The mechanical properties of the samples were tested by carrying out a tensile test. Tensile tests were performed in accordance with DIN EN ISO 527 using a Zwick Z1485 universal testing machine (ZwickRoell GmbH & Co. KG, Ulm, Germany). The specimens had dimensions corresponding to ISO 527-1A. Young's modulus of the annealed tensile bars was determined at a testing speed of 1 mm/min up to 0.25% elongation, followed by continued testing at 50 mm/min until specimen failure. For each material blend, a minimum of five specimens was tested to ensure statistical reliability of the results.

3 | Results and Discussion

3.1 | Molecular Weight

Gel permeation chromatography was used to characterize the molecular weight distribution of the PET blends. The resulting chromatograms enable conclusions to be drawn about the distribution of chain lengths and allow parameters such as the number-average molecular weight (M_n) and the weight-average molecular weight (M_w) to be determined. Figure 2a shows the results of gel permeation chromatography of PET blends and their unprocessed virgin components. The two blends 100/0 and 0/100 correspond to the pure virgin materials (IV 0.53 and IV 0.84), only processed with the twin-screw extruder. The molecular weight distributions of the blends lie between those of the pure components and shift depending on the mixing ratio. This shows how mixing PET grades with different molecular weights leads to a spectrum of materials with intermediate molecular weight distributions. Figure 2b shows the normalized RI signal over the retention volume obtained from the GPC measurement. This was measured for high- and low-molecular-weight virgin materials, a solvent-based blend and an extruded blend. Additionally, the theoretical sum of the two individual chromatograms at a ratio of 50:50 was calculated using the two virgin components. This represents what the blend would look like if there were no build-up or breakdown processes taking place. The actual measured unprocessed 50/50 mixture matches the calculated curve. This indicates that the molecular masses are not affected as a result of simple physical mixing. Comparing the curves before and after processing the 50/50 blend shows

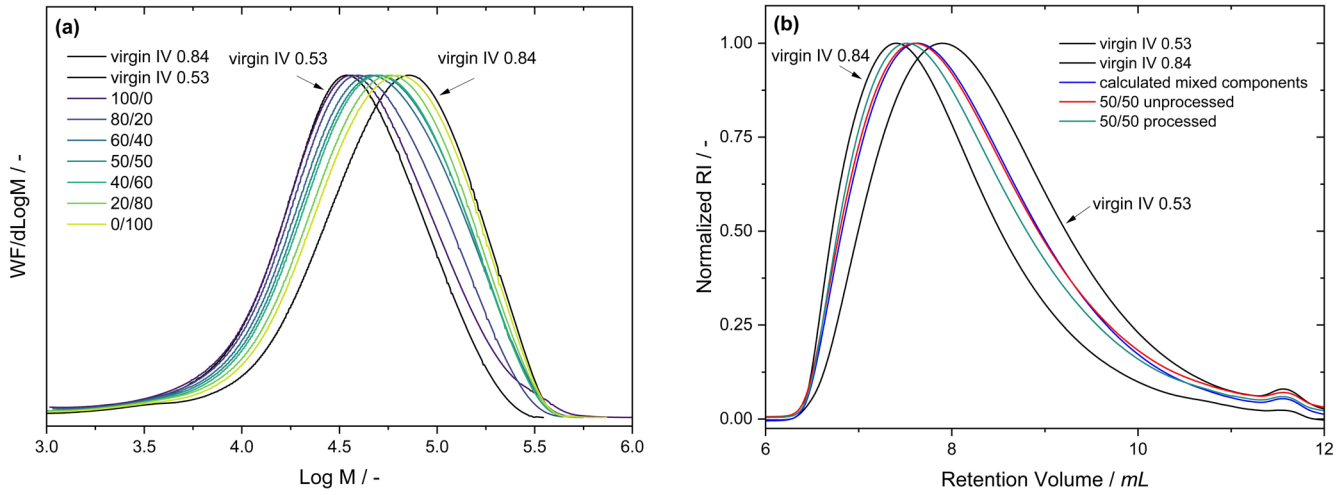

FIGURE 2 | (a) Molecular weight distribution of all blends and the low and high molecular weight virgin components determined by GPC. (b) GPC shows the normalized RI signal as a function of retention volume for the virgin components (IV 0.53 and IV 0.84), their theoretically calculated mixture, and the 50/50 blends in both unprocessed and processed states.

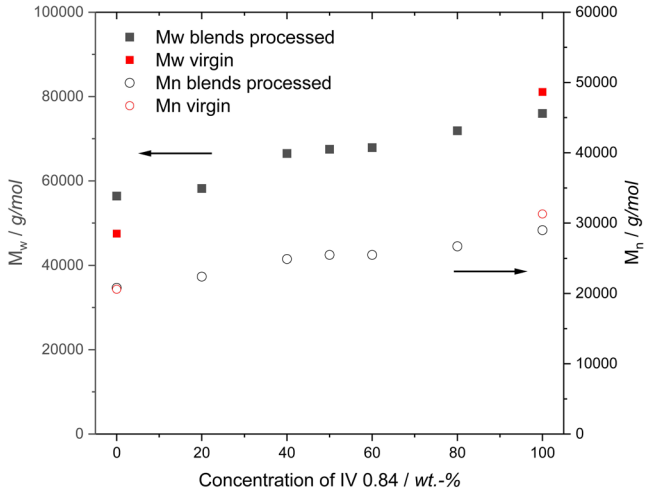

FIGURE 3 | Weight-average molecular weight (M_w, filled symbols, left *y*-axis) and number-average molecular weight (M_n, open symbols, right *y*-axis) of PET blends are shown as a plot against the concentration of the high molecular weight PET component (IV 0.84). Black symbols represent blends, red symbols neat components.

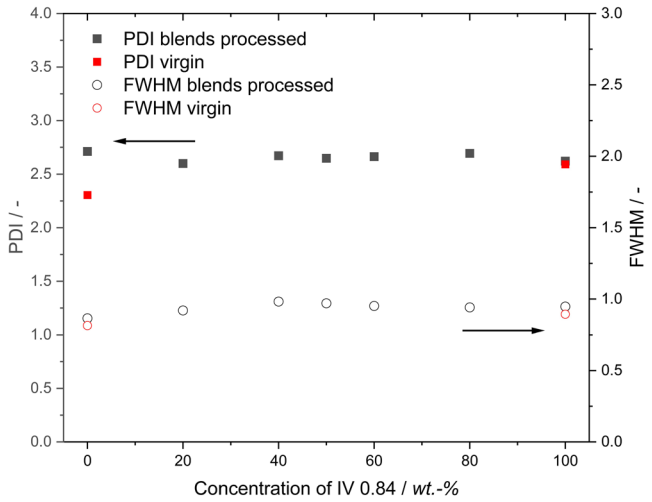

FIGURE 4 | Polydispersity Index (PDI, filled symbols, left *y*-axis) and Full Width at Half Maximum (FWHM, open symbols, right *y*-axis) of the molecular weight distribution of PET blends versus the concentration of the high molecular weight PET component (IV 0.84). Black symbols represent blends, red symbols neat components.

a shift towards lower retention volumes and a change in shape compared to the curve of the unprocessed blend. The processed 50/50 blend shows a slightly narrower elution peak and a slight shift towards longer polymer chains. More information can be found in Figure S11 of the Supporting Information. As demonstrated in Figure 3, both M_w and M_n increase linearly with the amount of high molecular weight PET (IV 0.84) in the blend.

A comparison of the molecular weights of processed neat materials (100/0 and 0/100 blends) with the virgin materials shows a decrease in the chain length of the high molecular weight PET, while the chain length of the low molecular weight PET increases. For the low IV component, the increase in M_w due to processing indicates polycondensation because this value is strongly affected by longer chains. However, M_n remains stable, showing that either the total number of chains remains largely unchanged or the fluctuations are below the resolution of the GPC measurement [46]. Kruse et al. have already demonstrated that the surrounding atmosphere influences the molecular weight of PET [47]. Degradation of the material occurs in the presence of air, resulting in a reduction of molecular weight. In contrast, polycondensation occurs in a nitrogen atmosphere, leading to an increase in molecular weight. The molecular weight of the polymer also has a significant effect on the thermal and thermo-oxidative degradation stability of PET [45]. Polyethylene terephthalate with a high molecular weight shows high thermal stability in a nitrogen atmosphere but low stability in air, which results in a high susceptibility to reduction in molecular weight, whereas PET with low molecular weight exhibits the lowest degradation rate. During processing, degradation and polycondensation are additionally influenced by shear stress and the number of reactive end groups. High molecular weight PET experiences higher shear stress during extrusion but has only a small number of end groups, resulting in low reactivity. Therefore, chain scission dominates, and the molecular weight decreases. In contrast, low molecular weight PET experiences lower shear stress and has a high number of reactive end groups. This favors polycondensation during processing, leading to an increase in molecular weight. The PET with the lowest molecular weight also has the highest number of hydroxyl end groups per molecule, which increases the potential for polycondensation reactions and thus also the reaction speed. With high molecular weight PET, the reaction rate is therefore also slower [45].

As there are both oxygen-rich and oxygen-poor areas in the extruder, chain scission as well as chain extension, branching, or even crosslinking occur during the extrusion of PET [48–50]. Depending on the molecular weight of the blend components, the molecular weight of the low IV PET is increased due to the polycondensation and the molecular weight of the high IV PET is reduced due to the degradation effects, which can be seen in Figure 3 when comparing the virgin materials and the 100/0 and 0/100 blends.

Additionally, the polydispersity index (PDI) can be calculated by dividing M_w by M_n. The full width at half maximum (FWHM) can be calculated using the molecular weight distribution. Both values provide information about the width of the molecular weight distribution. The higher the PDI and FWHM, the broader the distribution. Both values are shown as a function of a high molecular weight PET content in Figure 4. Neither the PDI nor the FWHM depends on the mixing ratio. It was expected that the molecular weight distribution would broaden as a consequence of the mixing of polymers with high and low molecular weights [51]. However, this cannot be seen in the measurement data.

A potential explanation for this finding could be the combination of an increase and a decrease in molecular weight during the extrusion process. Within the oxygen-rich region of the extruder, the molecular weight of high molecular weight PET is reduced due to its lower stability, while low molecular weight PET undergoes less degradation. In the low-oxygen areas of the extruder, however, the low molecular weight PET shows a high potential for polycondensation due to the high number

of hydroxyl end groups, which increases the molecular weight. The combination of these effects results in a shift of the molecular weight distributions of the blend components towards each other. This results in an averaging effect of the polymer chains. Consequently, the molecular weight distribution does not become broader. The corresponding results of the GPC analysis are summarized in Table 3.

3.2 | Thermal Properties

We performed differential scanning calorimetry (DSC) measurements to analyze the thermal properties of the mixtures. To ensure a consistent basis for comparison, all samples were subjected to a uniform heating and cooling protocol. Figure 5 presents the second heating scan and Figure 6 presents the cooling scan obtained from the DSC measurements.

Figure 5 shows the heat flow over the temperature range from 35°C to 295°C, with endothermic processes generating a positive peak and exothermic processes a negative peak. All PET blends show a step at approx. 80°C in the 2nd heating curve, which describes the glass transition temperature T_g. T_g is known to depend on the average molecular weight of the polymer [25]. No significant differences in T_g were found in the PET blends tested. A possible explanation for the similar T_g values for M_n can be attributed to the relatively small differences in molecular weight between the samples, which are insufficient to cause a measurable shift in the glass transition temperature.

In the range from 240°C to 260°C, all blends show an endothermic peak, which reflects the melting range of the crystalline components. The melting peak decreases with the content of the high molecular weight PET. These findings are also consistent with the literature, in which PET with a lower molecular weight forms more perfect and densely packed crystals, which require more energy, i.e., higher temperatures, to melt the polymer [21].

Looking at the degree of crystallinity of the blends, a decrease is observed as the percentage of the high molecular weight blend partner increases. This increase in molecular weight corresponds to the content of PET IV 0.84. The diffusion of longer macromolecular chains at the interface for crystal growth requires more energy, which in turn reduces the crystallization rate, decreases the total amount of crystalline phases, and increases the amount of amorphous phases [52].

Figure 6 shows the first cooling curves of the blends. There is an exothermic peak between 180°C and 210°C. This peak is caused by the crystallization of the polymer. As the amount of high molecular weight PET increases, the crystallization shifts to lower temperatures, and the crystallization peak becomes broader. This is due to the higher mobility of short polymer chains compared to longer polymer chains. The higher mobility increases the crystallization rate of the short polymer chains, resulting in a narrower exothermic peak at higher temperatures. As the proportion of high molecular weight PET increases, the crystallization rate decreases, resulting in a shift to lower temperatures and a broadening of the crystallization peak [20, 53, 54]. The corresponding thermal parameters are summarized in Table 4.

TABLE 3 | Values of weight-average molecular weight (M_w), number-average molecular weight (M_n), and polydispersity index (PDI) of the blends.

Blend (low M_w/ high M_w)	M_n (g/mol)	M_w (g/mol)	PDI
100/0	20,800	56,400	2.7
80/20	22,400	58,200	2.6
60/40	24,900	66,500	2.7
50/50	25,500	67,500	2.7
40/60	25,500	67,900	2.7
20/80	26,700	71,900	2.7
0/100	29,000	76,000	2.6

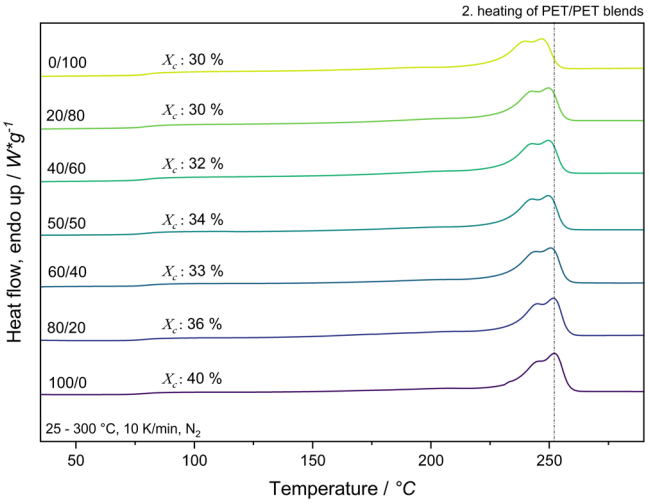

FIGURE 5 | DSC heating curve of PET blends with varying ratios of low and high molecular weight components. The compositions are indicated as low M_w/high M_w ratios. X_c values represent the degree of crystallinity.

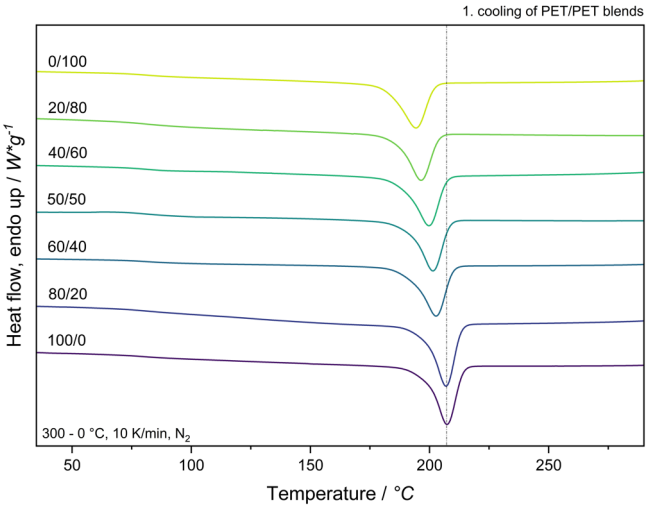

FIGURE 6 | DSC cooling curve of PET blends with varying ratios of low and high molecular weight components. The compositions are indicated as low M_w/high M_w ratios.

3.3 | Rheological Properties

To investigate the flow properties of the PET blends, shear oscillation rheological measurements were carried out under nitrogen atmosphere. The results are shown in Figure 7. In addition to the blends, the unprocessed blend components were also analyzed.

In the high frequency range, all samples show a decrease in complex viscosity with increasing frequency. This shear-thinning behavior is characteristic of polymer melts and indicates the dominance of disentanglement processes at higher shear rates. In the low-frequency range, all materials exhibit a Newtonian plateau at different levels depending on the molecular weight. As the proportion of the high molecular weight component increases, the viscosity increases. This is due to a higher average molecular weight, consequently resulting in a higher degree of chain entanglement. This observation is consistent with the GPC results. Also, the blends with lower molecular weight show an increase in viscosity during the measurement explainable by the high potential for polycondensation due to the high hydroxyl end group concentration [47].

Comparing the unprocessed, high molecular weight blend component IV 0.84 with the processed blend 0/100, the Newtonian plateau of the 0/100 blend is lower. This is due to thermal-oxidative and shear degradation during processing in the twin-screw extruder. However, comparing the low molecular weight blend component IV 0.53 with the processed blend 100/0 shows that the level of the Newtonian plateau increases during processing. These results of the rheological measurements, that high molecular weight PET tends to degrade, while low molecular weight PET tends to increase in molecular weight during the extrusion process due to the different oxygen concentrations, correspond very well with the GPC measurements and with the literature [45, 50].

Figure 8 shows the zero shear viscosities of PET polymer blends with high and low molecular weights in relation to the weight percentage of the high molecular weight blend component (IV 0.84). The experimental data are then compared with the values predicted by the logarithmic additivity rule, under the assumption of ideal mixing behavior without specific interactions.

According to the logarithmic additivity rule, the viscosity of a binary polymer blend can be estimated from the viscosities of the pure components using a logarithmic mixing relationship (Equation 2).

$$\ln \eta_{\text{blend}} = w_1 \cdot \ln \eta_1 + w_2 \cdot \ln \eta_2 \tag{2}$$

Here, η_{Blend} is the viscosity of the blend, η_1 and η_2 are the viscosities of the two pure components, and w_1 and w_2 are their respective weight fractions. The viscosities of the pure mixture components are also shown. The zero shear viscosities were determined by fitting the shear viscosity data to the Carreau-Yasuda model. To ensure an accurate fit and minimize the influence of running-in effects, the first measurement point at 1 rad/s was excluded from the model fitting.

TABLE 4 | Values of glass transition temperature T_g, peak of melting temperature T_m, peak of crystallization temperature T_c, and the degree of crystallinity of the blends.

Blend (low M_w/high M_w)	T_g (°C)	T_m (°C)	T_c (°C)	Degree of crystallinity (%)
100/0	80 ± 0	253 ± 0	208 ± 2	40 ± 2
80/20	80 ± 1	252 ± 1	206 ± 1	36 ± 0
60/40	80 ± 1	251 ± 0	203 ± 1	33 ± 1
50/50	80 ± 1	250 ± 0	202 ± 0	34 ± 1
40/60	80 ± 1	250 ± 0	200 ± 1	32 ± 1
20/80	80 ± 0	248 ± 0	197 ± 0	30 ± 1
0/100	81 ± 0	247 ± 0	194 ± 0	30 ± 0

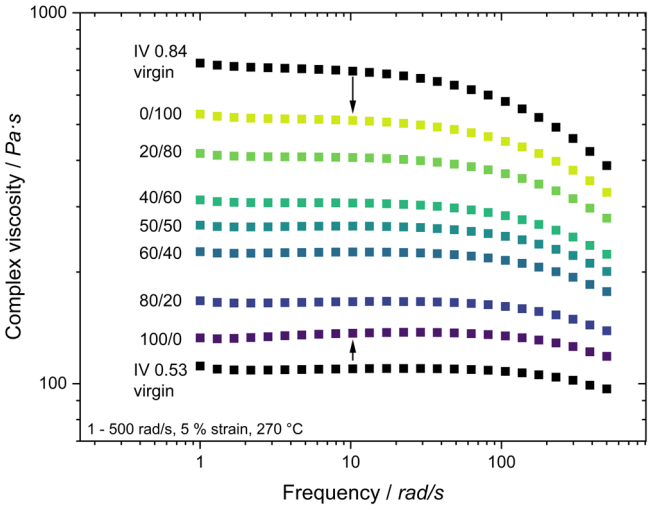

FIGURE 7 | Complex viscosity as a function of frequency for blends of low (IV 0.53) and high (IV 0.84) molecular weight PET materials at different ratios, including the virgin components, measured at 270°C and 5% strain.

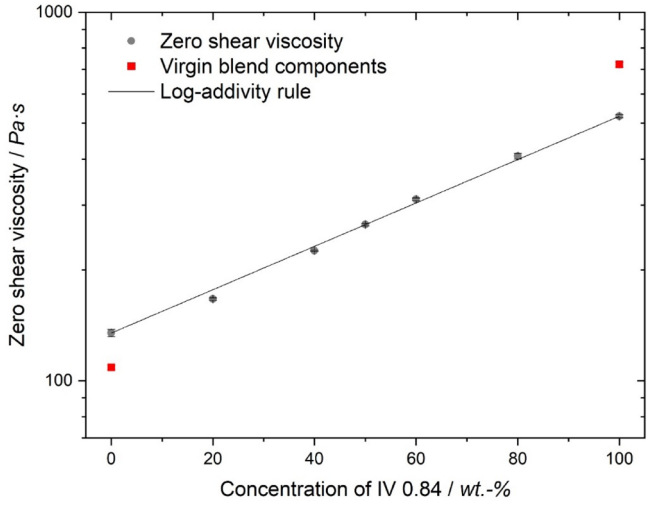

FIGURE 8 | Zero-shear viscosity of PET blends as plotted against the concentration of the high molecular weight component (IV 0.84). Experimental data for the blends are shown as gray circles, the log-additivity rule as a solid gray line and the zero-shear viscosities of the virgin blend components as red squares.

TABLE 5 | Mechanical properties (Young's Modulus, Tensile Strength, Elongation at break) presented as average values with sample standard deviations and degree of crystallinity after annealing for PET blends with varying ratios of low and high molecular weight components.

Blend (low M_w/high M_w)	Young's modulus (GPa)	Tensile strength (MPa)	Elongation at break (%)	Core degree of crystallinity after annealing (%)
100/0	3.360 ± 0.030	72.2 ± 4.2	2.7 ± 0.3	32
80/20	3.340 ± 0.020	83.7 ± 0.5	5.4 ± 0.7	31
60/40	3.300 ± 0.010	82.8 ± 0.5	8.6 ± 0.8	31
50/50	3.320 ± 0.020	82.4 ± 0.5	9.1 ± 0.5	29
40/60	3.230 ± 0.010	81.7 ± 0.3	6.0 ± 3.1	29
20/80	3.340 ± 0.010	82.8 ± 0.5	8.3 ± 0.5	29
0/100	3.370 ± 0.020	83.1 ± 0.4	8.2 ± 0.5	28

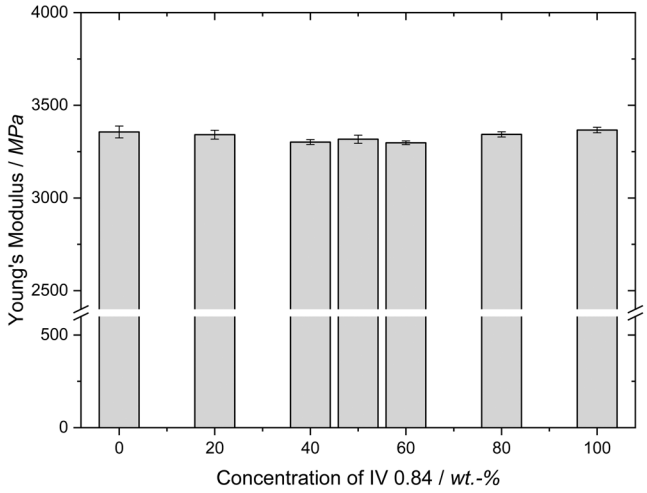

FIGURE 9 | Young's Modulus of PET blends plotted against the concentration of the high molecular weight component (IV 0.84). Error bars show the sample's standard deviation.

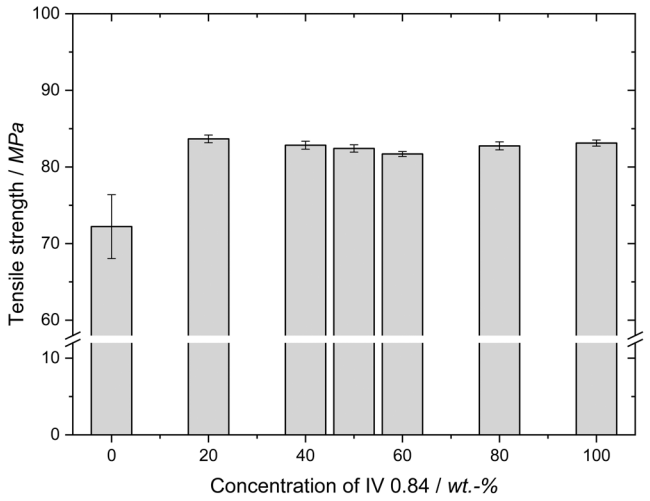

FIGURE 10 | Tensile strength of PET blends as a function of the concentration of the high molecular weight component (IV 0.84). Error bars show the sample's standard deviation.

The measured zero shear viscosities generally follow the logarithmic additivity rule, with an R^2 of 0.99, indicating an excellent correlation between experimental data and the predicted values.

3.4 | Mechanical Properties

Tensile tests were conducted to determine the mechanical properties of the blends. For this purpose, the materials were injection molded into standard test specimen geometry according to ISO 527-1A. As the degree of crystallinity significantly influences mechanical performance and can vary across the specimen cross-section due to differences in crystallization rates, a thermal post-treatment was applied [55]. To ensure homogeneous crystallinity distribution throughout the cross-section of the specimen, the tensile test specimens were annealed. As a result, crystallinity of the test specimen core in the range of 28%–32% was achieved for all blends. An overview of all the results of the mechanical analysis is shown in Table 5. Representative stress–strain curves for all blends can be found in Figures S12–S18 in the Supporting Information. The absence of strain hardening, a behavior typically observed in bimodal polyethylene systems, suggests that the molecular weight distribution in these PET blends does not induce similar reinforcement effects [56, 57].

Figure 9 shows the Young's modulus in relation to the amount of high molecular weight PET. All blends exhibit a similar Young's modulus, regardless of molecular weight. This observation is consistent with findings reported in the literature, which indicate that Young's modulus is largely independent of molecular weight and is instead primarily influenced by the degree of crystallinity [55, 58]. Since the degree of crystallinity remains approximately constant across the investigated blends, the Young's modulus shows little variation.

Figure 10 presents the tensile strength in relation to the proportion of high molecular weight blend partner. When the content of high molecular weight PET reaches 20 wt.% or more, the tensile strength reaches a plateau at approximately 83 MPa. In contrast, the blend containing 0 wt.% high molecular weight PET exhibited a significant decrease in tensile strength. These findings are consistent with the existing literature, which

documents an increase in tensile strength with molecular weight up to a certain threshold [58–60]. This behavior is attributed to the growing number of chain entanglements with increasing molecular weight, leading to the formation of a physical network. The entanglement molecular weight (Me) of PET ranges from 1180 to 2120 g/mol [61]. Above Me, the polymer chains are long enough to form entanglements. The PET blends investigated are well above this value. Beyond a certain molecular weight, however, further increases do not significantly enhance entanglement density, as the system has already reached a state of entanglement saturation. It should be noted that most existing studies were conducted using amorphous polymers, which allowed the influence of crystallinity to be ignored. As all blends have almost identical degrees of crystallinity, influences due to different degrees of crystallinity can be excluded. However, the semi-crystalline structural properties of the blends may vary [62]. In addition to molecular weight itself, the molecular weight distribution also plays a role in determining tensile strength. A broader distribution (i.e., higher polydispersity index, PDI) is generally associated with lower tensile strength, whereas a narrower distribution improves tensile strength [58, 59]. All blends analyzed have a very similar PDI, ensuring that differences in tensile strength can be attributed primarily to changes in molecular weight rather than distribution.

Figure 11 shows the tensile strength in relation to the amount present of the blend partner with a high molecular weight. An increase in the content of high molecular-weight PET results in an increase in elongation at break, indicating improved deformability. This behavior is attributed to the increased number of molecular chain entanglements associated with a higher molecular weight, which enhances the material's capabilities in terms of plastic deformation. A plateau is observed at a concentration of approximately 40 wt.% of high molecular weight PET. Beyond this concentration, a further increase in molecular weight does not significantly affect elongation at break. In addition to molecular weight, both polydispersity and degree of crystallinity are known to influence the elongation at break. However, for the samples investigated in this study, the polydispersity index and the degree of crystallinity remain approximately constant, allowing the observed effects to be attributed primarily to variations in molecular weight.

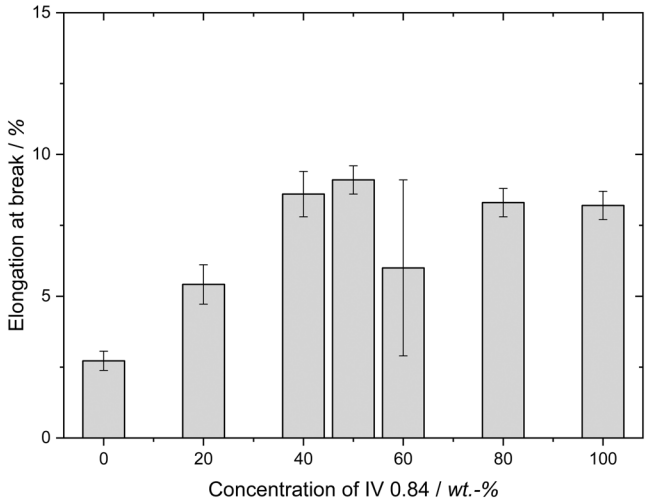

FIGURE 11 | Elongation at break of PET blends plotted against the concentration of the high molecular weight component (IV 0.84). Error bars show the sample's standard deviation.

4 | Conclusion

This study investigated monopolymer blends of PET with high and low molecular weight components to better understand structure–property relationships relevant to mechanical recycling. The molecular weight distribution, thermal, rheological and mechanical properties of these blends were systematically investigated. The results demonstrate that blending enables controlled tuning of molecular weight distribution, viscosity and mechanical performance. According to the GPC and rheological data, simultaneous chain scission and extension occur during extrusion, crucially leading to a convergence of molecular weights rather than a broadening of the molecular weight distribution, particularly in intermediate blend ratios. This observation is supported by the nearly constant PDI across all blends, which indicates that chain degradation and chain extension occur concurrently, resulting in a stable molecular weight distribution. This convergence is attributed to the fact that higher molecular weights tend to degrade more easily, while lower molecular weights are more prone to chain extension through polycondensation (in oxygen-poor regions). Although this study focuses on a fixed set of extrusion parameters, it is important to note that the kinetics of these competing reactions are affected by processing temperature and residence time. Therefore, investigating the effects of process parameters such as temperature, screw speed and throughput is a relevant and attractive future research, in order to gain a comprehensive and robust understanding of the dynamics of degradation and polycondensation. Thermal analysis shows a decrease in the degree of crystallinity and melting temperatures with increasing high molecular weight content, likely due to reduced chain mobility and hindered crystallization kinetics. Mechanical tests reveal that a moderate addition of high molecular weight PET ($\geq$ 20 wt.%) significantly increases tensile strength and elongation at break without affecting modulus, suggesting a threshold for entanglement-driven reinforcement.

These findings confirm that tailored blending strategies can compensate for molecular degradation in recycled PET without additives up to a certain point. In addition to blending strategies, post-consumer PET with reduced molecular weight can be further enhanced through solid-state polycondensation (SSP) or reactive extrusion with chain extenders, both of which are established methods to increase molecular weight and restore material performance. Furthermore, the customized rheological behavior achieved through blending expands the range of processing possibilities. The stability of molecular weight distribution, resulting from the interplay of degradation and chain extension, ensures consistent material properties, which is a key advantage for high-value applications.

Acknowledgments

This research was funded by the German Research Foundation (DFG), project number 518732456. Special thanks to Andreas Himmelsbach,

Ute Kuhn and Sebastian Gröschel for their support during the trials. Open Access funding enabled and organized by Projekt DEAL.

Funding

German Research Foundation (DFG), Grant/Award Number: RU 2586/9-1; Bayerischen Staatsministerium für Wissenschaft und Kunst, Project Number: 518732456.

Conflicts of Interest

The authors declare no conflicts of interest.

Data Availability Statement

The data that support the findings of this study are available from the corresponding author upon reasonable request.

References

1. A. L. Andrady and M. A. Neal, "Applications and Societal Benefits of Plastics," *Philosophical Transactions of the Royal Society of London. Series B, Biological Sciences* 364 (2009): 1977–1984.

2. S. E. Selke, J. D. Culter, R. A. Auras, and M. Rabnawaz, *Plastics Packaging* (Carl Hanser Verlag GmbH & Co. KG, 2021).

3. U. Bruder, *User's Guide to Plastic* (Hanser; Hanser Publications, 2019).

4. J. P. Jog, "Crystallization of Polyethyleneterephthalate," *Journal of Macromolecular Science, Part C: Polymer Reviews* 35 (1995): 531–553.

5. Plastics Europe, *Plastics – The Fast Facts 2024* (Plastics Europe, 2024), accessed on 1 February 2025, https://plasticseurope.org/knowledge-hub/plastics-the-fast-facts-2024/.

6. A. Eshkeiti, A. S. G. Reddy, S. Emamian, et al., "Screen Printing of Multilayered Hybrid Printed Circuit Boards on Different Substrates," *IEEE Transactions on Components, Packaging and Manufacturing Technology* 5 (2015): 415–421.

7. P. Sarda, J. C. Hanan, J. G. Lawrence, and M. Allahkarami, "Sustainability Performance of Polyethylene Terephthalate, Clarifying Challenges and Opportunities," *Journal of Polymer Science* 60 (2022): 7–31.

8. T. Çaykara, M. G. Sande, N. Azoia, L. R. Rodrigues, and C. J. Silva, "Exploring the Potential of Polyethylene Terephthalate in the Design of Antibacterial Surfaces," *Medical Microbiology and Immunology* 209 (2020): 363–372.

9. H. Limami, I. Manssouri, K. Cherkaoui, and A. Khaldoun, "Study of the Suitability of Unfired Clay Bricks With Polymeric HDPE & PET Wastes Additives as a Construction Material," *Journal of Building Engineering* 27 (2020): 100956.

10. G. G. N. Thushari and J. D. M. Senevirathna, "Plastic Pollution in the Marine Environment," *Heliyon* 6 (2020): e04709.

11. M. MacLeod, H. P. H. Arp, M. B. Tekman, and A. Jahnke, "The Global Threat From Plastic Pollution," in *Science*, vol. 373 (AAAS, 2021), 61–65.

12. J. Hopewell, R. Dvorak, and E. Kosior, "Plastics Recycling: Challenges and Opportunities," *Philosophical Transactions of the Royal Society of London. Series B, Biological Sciences* 364 (2009): 2115–2126.

13. M. M. Owen, E. O. Achukwu, A. M. Hazizan, A. Z. Romli, and U. S. Ishiaku, "Characterization of Recycled and Virgin Polyethylene Terephthalate Composites Reinforced With Modified Kenaf Fibers for Automotive Application," *Polymer Composites* 43 (2022): 7724–7738.

14. Y. Srithep, D. Pholharn, A. Dassakorn, and J. Morris, "Effect of Chain Extenders on Mechanical and Thermal Properties of Recycled Poly (Ethylene Terephthalate) and Polycarbonate Blends," *IOP Conference Series: Materials Science and Engineering* 213 (2017): 12008.

15. D. Y. Kim, T. H. Park, J. E. Choo, and S. W. Hwang, "Evaluation of PETrecyclability and Characterization of Modifiedreprocessed – PET for Industrial Application," *Journal of Applied Polymer Science* 141 (2024): 141.

16. R. Q. Albuquerque, F. Stephan, A. Pongratz, C. Brütting, K. Krause, and H. Ruckdäschel, "Recycling of Thermoplastics with Machine Learning: A Review," *Advanced Functional Materials* 36, no. 3 (2025): e09447.

17. H. Zimmerman and N. T. Kim, "Investigations on Thermal and Hydrolytic Degradation of Poly(Ethylene Terephthalate)," *Polymer Engineering and Science* 20 (1980): 680–683.

18. M. Paci and F. P. La Mantia, "Competition Between Degradation and Chain Extension During Processing of Reclaimed Poly(Ethylene Terephthalate)," *Polymer Degradation and Stability* 61 (1998): 417–420.

19. J. Scheirs and T. E. Long, *Modern Polyesters: Chemistry and Technology of Polyesters and Copolyesters* (Wiley, 2006).

20. M. Frounchi, "Studies on Degradation of PET in Mechanical Recycling," *Macromolecular Symposia* 144 (1999): 465–469.

21. J. Hatt, K. Englund, and H. Li, "Characterizing the Changes to the Material Properties of a Bottle-Grade Poly(Ethylene Terephthalate) Subject to Repeated Melt Extrusion," *Journal of Applied Polymer Science* 140 (2023): 140.

22. C. Helbig, J. Huether, C. Joachimsthaler, et al., "A Terminology for Downcycling," *Journal of Industrial Ecology* 26 (2022): 1164–1174.

23. F. La, P. Mantia, and F. Vinci, "Recycling Poly(Ethyleneterephthalate)," *Polymer Degradation and Stability* 45 (1994): 121–125.

24. J. D. Badia, E. Strömberg, S. Karlsson, and A. Ribes-Greus, "The Role of Crystalline, Mobile Amorphous and Rigid Amorphous Fractions in the Performance of Recycled Poly (Ethylene Terephthalate) (PET)," *Polymer Degradation and Stability* 97 (2012): 98–107.

25. L.-P. Blanchard, J. Hesse, and S. L. Malhotra, "Effect of Molecular Weight on Glass Transition by Differential Scanning Calorimetry," *Canadian Journal of Chemistry* 52 (1974): 3170–3175.

26. R. Wei and W. Zimmermann, "Microbial Enzymes for the Recycling of Recalcitrant Petroleum-Based Plastics: How Far Are We?," *Microbial Biotechnology* 10 (2017): 1308–1322.

27. S. Yoshida, K. Hiraga, T. Takehana, et al., "A Bacterium That Degrades and Assimilates Poly(Ethylene Terephthalate)," in *Science*, vol. 351 (AAAS, 2016), 1196–1199.

28. W. Zimmermann, "Biocatalytic Recycling of Polyethylene Terephthalate Plastic," *Philosophical Transactions. Series A, Mathematical, Physical, and Engineering Sciences* 378 (2020): 20190273.

29. T. Menzel, S. Weigert, A. Gagsteiger, et al., "Impact of Enzymatic Degradation on the Material Properties of Poly(Ethylene Terephthalate)," *Polymers* 13 (2021): 13.

30. A. Bohre, P. R. Jadhao, K. Tripathi, K. K. Pant, B. Likozar, and B. Saha, "Chemical Recycling Processes of Waste Polyethylene Terephthalate Using Solid Catalysts," *ChemSusChem* 16 (2023): e202300142.

31. A. Carniel, V. d. A. Waldow, and A. M. de Castro, "A Comprehensive and Critical Review on Key Elements to Implement Enzymatic PET Depolymerization for Recycling Purposes," *Biotechnology Advances* 52 (2021): 107811.

32. K. Ragaert, L. Delva, and K. van Geem, "Mechanical and Chemical Recycling of Solid Plastic Waste," in *Waste Management*, vol. 69 (Elsevier, 2017), 24–58.

33. R. Scaffaro and F. P. La Mantia, "Characterization of Monopolymer Blend of Virgin and Recycled Polyamide 6," *Polymer Engineering and Science* 42 (2002): 2412–2417.

34. M. Rahimi, M. Esfahanian, and M. Moradi, "Effect of Reprocessing on Shrinkage and Mechanical Properties of ABS and Investigating the Proper Blend of Virgin and Recycled ABS in Injection Molding," *Journal of Materials Processing Technology* 214 (2014): 2359–2365.

35. I. Hamarat, E. Kuram, and B. Ozcelik, "Investigation of the Mechanical, Rheological, and Morphological Properties of Acrylonitrile Butadiene Styrene Blends With Different Recycling Number Content," *Proceedings of the Institution of Mechanical Engineers, Part E: Journal of Process Mechanical Engineering* 232 (2018): 449–458.

36. F. P. La Mantia, M. C. Mistretta, and V. Titone, "An Additive Model to Predict the Rheological and Mechanical Properties of Polypropylene Blends Made by Virgin and Reprocessed Components," *Recycling* 6 (2021): 2.

37. D.-M. Fann, S. K. Huang, and J.-Y. Lee, "Kinetics and Thermal Crystallinity of Recycled PET. I. Dynamic Cooling Crystallization Studies on Blends Recycled With Engineering PET," *Journal of Applied Polymer Science* 61 (1996): 1375–1385.

38. J. H. Lee, K. S. Lim, W. G. Hahm, and S. H. Kim, "Properties of Recycled and Virgin Poly(Ethylene Terephthalate) Blend Fibers," *Journal of Applied Polymer Science* 128 (2012): 1250–1256.

39. A. Elamri, A. Lallam, O. Harzallah, and L. Bencheikh, "Mechanical Characterization of Melt Spun Fibers From Recycled and Virgin PET Blends," *Journal of Materials Science* 42 (2007): 8271–8278.

40. G. G. Marques, A. Couffin, P. Hajji, R. Inoubli, V. Bounor-Legaré, and R. Fulchiron, "A Review on the Formulation and Rupture Properties of Polyethylene Terephthalate in a Mechanical Recycling Context," *Industrial and Engineering Chemistry Research* 63 (2024): 887–920.

41. H. Potente, M. Bastian, and J. Flecke, "Design of a Compounding Extruder by Means of the SIGMA Simulation Software," *Advances in Polymer Technology* 18 (1999): 147–170.

42. B. Wunderlich, ed., *Thermal Analysis* (Academic Press, 1992).

43. P. J. Carreau, D. C. de Kee, and R. P. Chhabra, *Rheology of Polymeric Systems: Principles and Applications* (Carl Hanser Verlag GmbH & Co. KG, 2021).

44. W. P. Cox and E. H. Merz, "Correlation of Dynamic and Steady Flow Viscosities," *Journal of Polymer Science* 28 (1958): 619–622.

45. M. Kruse and M. H. Wagner, "Time-Resolved Rheometry of Poly(Ethylene Terephthalate) During Thermal and Thermo-Oxidative Degradation," *Rheologica Acta* 55 (2016): 789–800.

46. I. M. Ward, *Mechanical Properties of Solid Polymers* (Wiley, 2013).

47. M. Kruse, V. H. Rolón-Garrido, and M. H. Wagner, "Rheological Characterization of Degradation and Polycondensation of Poly(Ethylene Terephthalate) Melt in Air and in Nitrogen," *AIP Conference Proceedings* 1526 (2013): 216–229.

48. L. K. Nait-Ali, X. Colin, and A. Bergeret, "Kinetic Analysis and Modelling of PET Macromolecular Changes During Its Mechanical Recycling by Extrusion," *Polymer Degradation and Stability* 96 (2011): 236–246.

49. R. Assadi, X. Colin, and J. Verdu, "Irreversible Structural Changes During PET Recycling by Extrusion," *Polymer* 45 (2004): 4403–4412.

50. Z. O. Schyns, A. D. Patel, and M. P. Shaver, "Understanding Poly(Ethylene Terephthalate) Degradation Using Gas-Mediated Simulated Recycling," *Resources, Conservation and Recycling* 198 (2023): 107170.

51. H.-W. Shen, B.-H. Xie, W. Yang, and M.-B. Yang, "Thermal and Rheological Properties of Polyethylene Blends With Bimodal Molecular Weight Distribution," *Journal of Applied Polymer Science* 129 (2013): 2145–2151.

52. L. Baldenegro-Perez, D. Navarro-Rodriguez, F. Medellin-Rodriguez, B. Hsiao, C. Avila-Orta, and I. Sics, "Molecular Weight and Crystallization Temperature Effects on Poly(Ethylene Terephthalate) (PET) Homopolymers, an Isothermal Crystallization Analysis," *Polymers* 6 (2014): 583–600.

53. M. Asensio, K. Nuñez, J. Guerrero, M. Herrero, J. C. Merino, and J. M. Pastor, "Rheological Modification of Recycled Poly(Ethylene Terephthalate): Blending and Reactive Extrusion," *Polymer Degradation and Stability* 179 (2020): 109258.

54. N. Kumar Barman, S. S. Bhattacharya, and A. A. Mandot, "Influence of Blending Proportion on Properties of Melt Spun Monofilaments Produced from Virgin PET and Recycled PET Blend," In *Proceedings of the International Conference on Green Technologies for Sustainable Development (GTSD2021)* (Dharamsinh Desai University, 2021).

55. A. Galeski, "Strength and Toughness of Crystalline Polymer Systems," *Progress in Polymer Science* 28 (2003): 1643–1699.

56. C. Long, Z. Dong, X. Liu, et al., "Simultaneous Enhancement in Processability and Mechanical Properties of Polyethylenes via Tuning the Molecular Weight Distribution From Unimodal to Bimodal Shape," *Polymer* 258 (2022): 125287.

57. T. Kida, R. Tanaka, Y. Hiejima, K. Nitta, and T. Shiono, "Improving the Strength of Polyethylene Solids by Simple Controlling of the Molecular Weight Distribution," *Polymer* 218 (2021): 123526.

58. H. W. McCormick, F. M. Brower, and L. Kin, "The Effect of Molecular Weight Distribution on the Physical Properties of Polystyrene," *Journal of Polymer Science* 39 (1959): 87–100.

59. J. R. Martin, J. F. Johnson, and A. R. Cooper, "Mechanical Properties of Polymers: The Influence of Molecular Weight and Molecular Weight Distribution," *Journal of Macromolecular Science, Part C: Polymer Reviews* 8 (1972): 57–199.

60. J. H. Golden, B. L. Hammant, and E. A. Hazell, "Degradation of Polycarbonates. IV. Effect of Molecular Weight on Flexural Properties," *Journal of Polymer Science, Part A: General Papers* 2 (1964): 4787–4794.

61. J. H. Youk, W. H. Jo, and D. I. Yoo, "Molecular Dimensions of Poly(Ethylene Isophthalate) and Poly(Ethylene Naphthalene-2,6-Dicarboxylate)," *Polymer Bulletin* 39 (1997): 257–263.

62. R. Popli and L. Mandelkern, "Influence of Structural and Morphological Factors on the Mechanical Properties of the Polyethylenes," *Journal of Polymer Science Part B: Polymer Physics* 25 (1987): 441–483.

Supporting Information

Additional supporting information can be found online in the Supporting Information section. **Figure S1:** Technical description of screw element. **Figure S2:** Technical description of screw element. **Figure S3:** Technical description of screw element. **Figure S4:** Technical description of screw element. **Figure S5:** Technical description of screw element. **Figure S6:** Technical description of screw element. **Figure S7:** Technical description of screw element. **Figure S8:** Technical description of screw element. **Figure S9:** Technical description of screw element. **Figure S10:** Technical description of screw element. **Figure S11:** Normalized RI signals as a function of retention volume for virgin PET components with different intrinsic viscosities (IV 0.53 and 0.84), their unprocessed and processed 50/50 blend, and the calculated theoretical mixture. **Figure S12:** Stress–strain curve of 100/0 blend. **Figure S13:** Stress–strain curve of 80/20 blend. **Figure S14:** Stress–strain curve of 60/40 blend. **Figure S15:** Stress–strain curve of 50/50 blend. **Figure S16:** Stress–strain curve of 40/60 blend. **Figure S17:** Stress–strain curve of 20/80 blend. **Figure S18:** Stress–strain curve of 0/100 blend. **Table S1:** Calculated values of retention volume width at different percentages of the maximum RI signal.